JREE: Vol. 5, No. 1, (Winter 2018) 23-34

Journal of Renewable Energy and Environment

Research Article

Journal Homepage: www.jree.ir

Parametric Assessment of a Novel Geothermal Multi-Generation Equipped with Dual-Organic Rankine Liquefied Natural Gas Regasification Cycle Using Advanced Exergy and Exergoeconomic-Based Analyses

Hediyeh Safari, Fatemeh Ahmadi Boyaghchi*

Department of Mechanical Engineering, Faculty of Engineering & Technology, Alzahra University, Deh-Vanak, Tehran, Iran.

P A P E R I N F O

Paper history:
Received 11 November 2018
Accepted in revised form 20 February 2019

Keywords:
Geothermal Energy
Dual-ORC
Hydrogen Production
Advanced Exergy
Advanced Exergoeconomic

A B S T R A C T

This research is concerned with the design and analysis of a geothermal based multi-generation system by applying both conventional and advanced exergy and exergoeconomic concepts. The proposed energy system consists of a dual-organic Rankine cycle (ORC) to vaporize liquefied natural gas (LNG) and produce electricity. A proton exchange membrane (PEM) electrolyzer is employed to produce hydrogen by receiving the power and coolant heat waste of dual ORC. Moreover, cooling effect is produced during LNG regasification by utilizing the cryogenic energy of LNG. Parametric studies are conducted to assess the effects of substantial input parameters, namely turbine 1 inlet pressure, mass rate of upper cycle, geothermal mass flow rate, on the various parts of exergy destruction and cost rates within the major components.

1. INTRODUCTION

Recently, the conventional exergy and exergoeconomic-based performance assessments of multi-generation systems have been of particular interest for various researchers. Ratlamwala et al. [1] proposed and modeled a novel multi-generation integrated, geothermal-based from the viewpoints of exergy and exergoeconomic concepts. Coskun et al. [2] investigated geothermal energy based multi-generation systems thermodynamically with seven different combinations for practical applications. The desired systems were examined under two distinct main groups for heating and cooling periods. Ozturk and Dincer [3] performed an exergy analysis of a solar-based multi-generation energy production system which produced power, heating, cooling, hot water, hydrogen and oxygen. Ratlamwala and Dincer [4] developed a new integrated geothermal based system, comprising of quadruple flash power plant, quadruple effect absorption cooling system, PEM and air conditioning process (cooling with dehumidification) for building applications. An optimization study was also performed to find the highest possible exergy efficiency and the lowest possible exergy destruction of the hextuple generation system. Al-Ali and Dincer [5] proposed a new multi-generational integrated geothermal-solar system for industrial use. Energy and exergy analyses were conducted to show the performance of the system and compare the results of single generation, cogeneration, tri-generation and multi-generation systems. The energy efficiency for the multi generation system was found higher than that of the single-generation system. Suleman et al. [6] proposed a new solar-geothermal energy based system for multi-generation applications, which consists of two ORCs for power generation. Parametric studies were performed to observe the effects of various parameters namely inlet pressure and temperature of the ORC turbine. Malik et al. [7] developed and studied energetically and exergetically a biomass-geothermal energy based multi-generation system involving ORC an industrial dryer and power. Also, the variations in exergy efficiencies and exergy destructions for the system components were determined with respect to changes in the reference-environment temperature and other major system parameters. Khalid et al. [8] analyzed thermodynamically a biomass and solar integrated system for multi-generation to deliver power, cooling, hot water, heated air. Panchal et al. [9] designed and developed a solar driven and geothermal driven multi-generation system to produce power, cooling effect, dry products, useful heat from the condenser of ORC, and other useful heat out from heat exchangers. The overall energy and exergy efficiencies of the single generation and multi-generation systems were studied. In addition, parametric studies were conducted to observe the effects of different substantial parameters on the performance of overall system. Almahdi et al. [10] studied energetically and exergetically a multi-generation system based on solar thermal energy including the hot and cold thermal storage in order to make it suitable to operate during the night. The proposed system was undertaken to deliver electricity, a heating effect, a cooling effect, hydrogen,

*Corresponding Author's Email: fahmadi@alzahra.ac.ir (F. Ahmadi Boyaghchi)

and dry sawdust biomass. In this regard, a novel renewable based multi-generation involving ORC, magnetic refrigeration cycle PEM electrolyzer and date dryer were developed to produce power, heating load, refrigeration, hydrogen, oxygen and dried date, simultaneously. The proposed system was analyzed using exergy and exerdoeconomic concepts. The performances of the system were evaluated by varying the substantial design parameters [11].

Boyaghchi and Chavoshi [12] designed a multi-generation energy system containing dual ORC, a biomass gasification process and a PEM electrolyzer to produce syngas, power, cooling load, hydrogen and oxygen. The exergetic and economic performances of the desired system were assessed through the parametric study for several working fluids.

A conventional exergetic analysis identifies irreversibilities within each component of a plant and exergoeconomic analysis estimates the costs related to the irreversibilities [13, 14]. Conventional analyses cannot provide any information about the interaction between components and real improvement potential of an energy system. This weakness is solved by advanced exergy and exergoeconomic analyses [15-17]. Advanced analyses determine which part is of the inefficiencies and the related costs are caused by component interactions and which part can be avoided through technological improvements of a plant. These analyses explicitly identify the exergy destruction and costs and separate them into two main groups: (1) avoidable-unavoidable exergy destruction/cost and (2) endogenous-exogenous exergy destruction/cost [18]. Several researches have been focused on using both advanced exergy and exergoeconomic analyses to identify the various components of exergy destruction and corresponding cost rate within the component of energy systems. For instance, Asgari et al. [19] analyzed an auto cascade ejector enhanced refrigeration cycle based on advanced exergy and exergoeconomic concepts. Sensitivity study was carried out to assess the variation of exergetic and economic improvement potentials; namely, total avoidable exergy destruction, total avoidable exergy destruction cost and total avoidable investment cost rates to the compressor mass flow rate, condenser, refrigerator evaporator and freezer evaporator inlet temperatures. Parametric study indicated that the condenser inlet temperature growth improves the total avoidable exergy destruction within 88.19 % [19].

Mehrpooya and Mousavi [20] used advanced exergy to investigate the irreversibility costs and investment costs rate for a solar-driven Kalina cycle. Advanced exergy analyses demonstrated that absorber (1.3 $/h) has the highest and lowest exergy destruction cost rate about 1.3 $/h. Also the results showed that turbine and separator have the highest and lowest exergoeconomic factor of 85.88 % and 1.105 %, respectively.

Khosravi et al. [21] evaluated the advanced exergy and advanced exergoeconomic analyses of an ORC. The advanced exergy analysis indicated that the heat recovery steam generator and turbine components are important to be improved based on exergetic performance.

This research aims to develop and assess a new integrated geothermal energy based multi-generation system which produces vaporized LNG, hydrogen, power and cooling effect for the first time. Advanced exergy and exergoeconomic analyses are performed to identify the most influential components and assess the real exergy and economic improvement potentials of the desired system. Parametric studies are also carried out to observe the effects of various substantial parameters namely turbine 1 inlet pressure, mass rate of upper cycle, geothermal mass flow rate in order to assess the variations of different exergy destruction and cost rates subdivisions within the components.

2. SYSTEM DISCRIPTION

Fig. 1 illustrates the schematic diagram of the proposed multi-generation. The main part of the desired system contains the two-stage ORC to vaporize LNG and produce electricity. Both cycles are driven by hot brine extracted from the geothermal well. R227 and R116 are selected as the best working fluids respectively in the top and bottom cycles [23]. The high pressure liquid leaving the pump (stream 2) passes through the heat exchanges 1B and 1A and absorbs heat from the hot brine. Superheated R227 enters the turbine 1 to generate power. The low pressure stream is led to the heat exchanger 1C to warm R116 in the bottom cycle and then passes through the condenser 1 to be liquefied by LNG.

In the bottom cycle, the high pressure R116 liquid (stream 8) is pre-heated by heat recovered from the exhaust flow of the turbine 2 (stream 12) in the heat exchanger 2B and then absorbs heat from the exhaust flue and the brine via the heat exchangers 1C and 2A (streams 9-10-11), respectively. The superheated stream is led to the turbine 2 to generate power. The low pressure R116 leaving the turbine 2 passes through the heat exchanger 2B to recycle the heat energy of the exhaust flue of the turbine 2. LNG regasification process contains streams L-1, L-2, L-3 and L-4. The low temperature LNG (stream L-1) heats and evaporates in the condensers 2 and 1, respectively and produces cooling effect in the condenser 2C in order to meet the fuel conditions. The desired system is equipped with PEM to produce hydrogen. The required water temperature is provided by a portion of the brine (stream G_5) in the heat exchanger 3A and its electricity is provided by the turbines output power.

3. METHODOLOGY

The mass and energy balances are applied to model the system components. To simplify thermodynamic model, the following assumptions are considered [22, 24]:

- All processes are steady state and steady flow with negligible potential and kinetic energy effects, and the heat loss in pipe lines is neglected.
- The reference conditions are considered as T_0 = 15 ^oC and P_0 = 101.325 kPa.
- The fluid leaving the condenser is saturated water.

- The thermodynamic properties of the working fluids are calculated by using the Engineering Equation Solver (EES) software.
- The LNG which is used in the cycle amassed to be methane.
- Net output power in all exergy and advanced exergy have been fixed as $\dot{W}_{net} = 2.3$ (MW).
- PEM electrolyzer working pressure is P = 101.325 kPa [6].

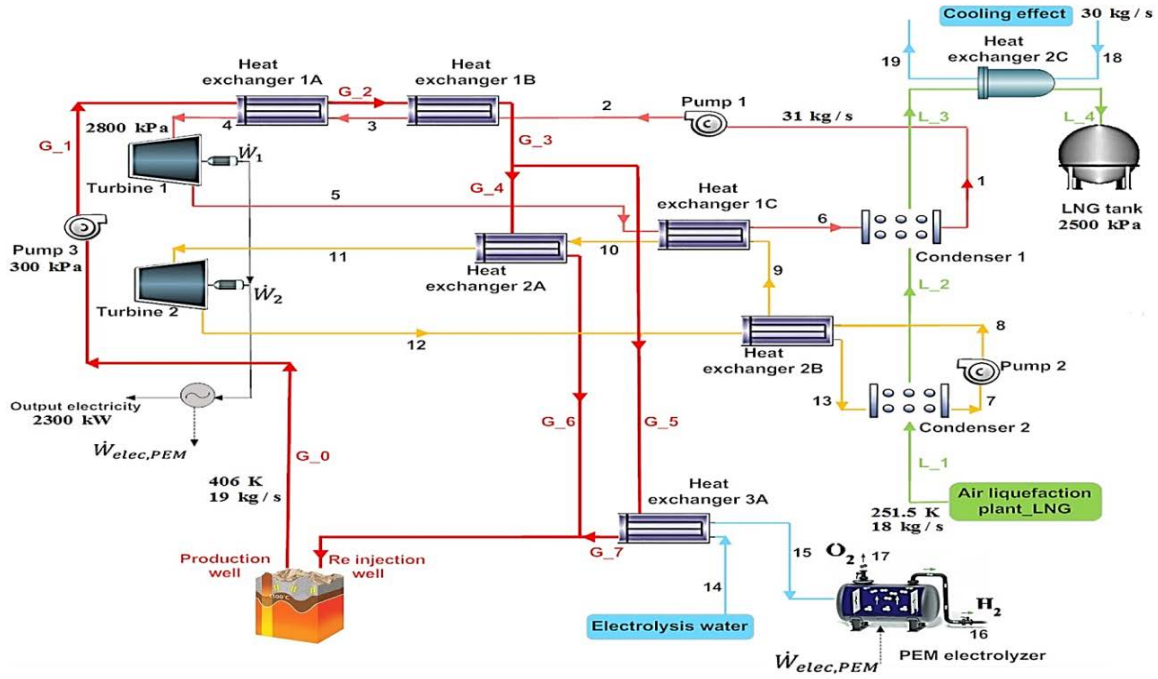

Figure 1. A schematic of the proposed multi-generation system.

3.1. Electrolyzer modeling

During the electrochemical reactions in PEM electrolyzer, electricity and heat are applied to split water into hydrogen and oxygen. The liquid water flows into the heat exchanger 3A and warms up to the PEM electrolyzer temperature. The H_2 produced at the cathode and the oxygen gas produced at the anode reject heat to the environment and cools to the reference environment temperature. In this work, thermochemical modeling is performed for the PEM electrolyzer. The total energy required by the electrolyzer can be calculated as [6, 22]:

$$\Delta H = \Delta G + T\Delta S \quad (1)$$

where ΔG and $T\Delta S$ represent Gibb's free energy and the thermal energy requirement, respectively. The values of G, S, and H for hydrogen, oxygen and water can be obtained from thermodynamic tables. The molar mass flow rate of hydrogen is determined by [6, 25]:

$$\dot{N}_{H_2,out} = \frac{J}{2F} \quad (2)$$

In Eqs. (2) and (3), J indicates the current density and F represents the Faraday constant. The PEM electrolyzer voltage can be expressed as:

$$V = V_0 + V_{act,a} + V_{act,c} + V_{ohm} \quad (3)$$

where V_0 is the reversible potential and can be obtained with the Nernst equation as follows:

$$V_0 = 1.229 - 8.5\times10^{-4}(T_{PEM} - 298) \quad (4)$$

In Eq. (5), $V_{act,a}$, $V_{act,c}$ and V_{ohm} indicate the anode activation overpotential, the cathode activation overpotential, and the electrolyte ohmic overpotential, respectively. Ohmic overpotential in PEM is caused by the membrane resistance to the hydrogen ions transported through it. The local ionic conductivity $\sigma(x)$ of PEM is expressed as:

$$\sigma_{PEM}[\lambda(x)] = (0.5139\lambda(x) - 0.326)\times\exp\left[1268\times\left(\frac{1}{303} - \frac{1}{T}\right)\right] \quad (5)$$

Here, $\lambda(x)$ is the water content in the membrane at a location x, i.e. distance into the membrane measured from the cathode- membrane interface. The overall ohmic resistance and the ohmic overpotential can thus be calculated by Eqs. (6) and (7):

$$R_{PEM} = \int_0^D \frac{dx}{\sigma_{PEM}[\lambda(x)]} \quad (6)$$

$$V_{ohm} = JR_{PEM} \quad (7)$$

The activation overpotential differentiated from the concentration of the oxidized and reduced species can be expressed as:

$$V_{act} = \frac{RT}{F}\sinh^{-1}\left(\frac{J}{2J_{0,i}}\right) \quad i = a, c \quad (8)$$

$$J_{0,i} = J_i^{ref} \exp\left(-\frac{V_{act,i}}{RT}\right) \quad i = a, c \tag{9}$$

where, J_0 is the exchange current density characterizing the capabilities of electrode in the electrochemical reaction. i and $V_{act,\ i}$ are the pre-exponential factor and the activation energy for the anode and cathode, respectively.

3.2. Conventional exergy and exergoeconomic analyses

Unlike energy analysis, an exergy analysis determines and identifies the irreversibilities in an enegy system. The total exergy associated with the ith material stream indicate the sum of the physical and chemical exergies. Since no chemical reaction occurs within the components of the desired system, only the physical exergy $\dot{E}x_i^{PH}$ associated with the ith material stream is considered [19]:

$$\dot{E}x_i^{PH} = \dot{m}_i.ex_i^{PH} = \dot{m}\left[(h_i - h_0) - T_0(s_i - s_0)\right] \tag{10}$$

Here, the subscript 0 stands for the property values at temperature T_0 and pressure P_0 of the reference state.

In Eq. (10), the point x (T_0, p) is defined at the given pressure p of the ith stream and the temperature T_0 of the environment.

The exergy destruction rate within the kth component of the system can be calculated as [19]:

$$\dot{E}x_{D,k} = \dot{E}x_{F,k} - \dot{E}x_{P,k} \tag{11}$$

In Eq. (12), $\dot{E}x_{P,k}$ and $\dot{E}x_{F,k}$ represent, respectively, the exergy of product and fuel for the kth component.

The cost balance of the kth component is:

$$\dot{C}_{P,k} = \dot{C}_{F,k} + \dot{Z}_k^{tot} \tag{12}$$

Here, $\dot{C}_{P,k}$ and $\dot{C}_{F,k}$ indicate the product and fuel cost rates within the k^{th} component and $\dot{Z}_k^{tot}$ shows the cost rate associated with the operating and maintenance and capital investment.

3.3. Advanced exergy and exergoeconomic analyses

The endogenous exergy destruction rate of the k^{th} component ($\dot{E}x_{D,k}^{EN}$) caused by the irreversibilites of the component itself can be calculated when it operates under real conditions [26], while all other components operate theoretically (as shown in Table 1). The exogenous exergy destruction rate of the kth component ($\dot{E}x_{D,k}^{EX}$) due to the irreversibilities of other components is calculated by subtracting the exogenous part of the exergy destruction rate from the real one.

$$\dot{E}x_{D,k}^{EX} = \dot{E}x_{D,k} - \dot{E}x_{D,k}^{EN} \tag{13}$$

The unavoidable exergy destruction rate of the k^{th} component ($\dot{E}x_{D,k}^{UN}$) indicating the technological and economic limitations of the component is estimated by applying the assumptions based on [27, 28] as listed in Table 1.

$$\dot{E}x_{D,k}^{UN} = \dot{E}x_{P,k}\left(\frac{\dot{E}x_{D,k}}{\dot{E}x_{P,k}}\right)^{UN} \tag{14}$$

The avoidable part of the exergy destruction rate for the k^{th} component ($\dot{E}x_{D,k}^{AV}$) representing the improvement potential of the desired component can be calculated as follows [27, 28]:

$$\dot{E}x_{D,k}^{AV} = \dot{E}x_{D,k} - \dot{E}x_{D,k}^{UN} \tag{15}$$

The unavoidable endogenous exergy destruction rate of the k^{th} component ($\dot{E}x_{D,k}^{UN,EN}$) and the unavoidable Exogenous one ($\dot{E}x_{D,k}^{UN,EX}$) are calculated as follows [22]:

$$\dot{E}x_{D,k}^{UN,EN} = \dot{E}x_{P,k}^{EN}\left(\frac{\dot{E}x_{D,k}}{\dot{E}x_{P,k}}\right)^{UN} \tag{16}$$

$$\dot{E}x_{D,k}^{UN,EX} = \dot{E}x_{D,k}^{UN} - \dot{E}x_{D,k}^{UN,EN} \tag{17}$$

The avoidable endogenous exergy destruction rate of the kth component ($\dot{E}x_{D,k}^{AV,EN}$) and the avoidable exogenous part ($\dot{E}x_{D,k}^{AV,EX}$) are calculated as follows [22]:

$$\dot{E}x_{D,k}^{AV,EN} = \dot{E}x_{D,k}^{EN} - \dot{E}x_{D,k}^{UN,EN} \tag{18}$$

$$\dot{E}x_{D,k}^{AV,EX} = \dot{E}x_{D,k}^{AV} - \dot{E}x_{D,k}^{AV,EN} \tag{19}$$

Similar to the advanced exergy analysis, the investment cost and the cost of exergy destruction rates can be divided into two endogenous and exogenous parts. The endogenous and the exogenous parts of the investment cost and the cost of the exergy destruction rates indicate the internal operating conditions and the interaction among the components, respectively [29].

The endogenous parts of exergy destruction and investment cost rates of the kth component can be calculated by Eqs. (20) and (21), respectively when the component operates under real conditions (Table 1) and all other components operate theoretically [30-32].

$$\dot{C}_{D,k}^{EN} = c_{F,k}^{real}\dot{E}x_{D,k}^{EN} \tag{20}$$

$$\dot{Z}_k^{EN} = Ex_{P,k}^{EN}\left(\frac{\dot{Z}}{\dot{E}x_P}\right)^{real} \tag{21}$$

The exogenous subdivisions of cost rates within the kth component which are due to the remaining system components are calculated by Eqs. (22) and (23) [30-32]:

$$\dot{C}_{D,k}^{EX} = \dot{C}_{D,k}^{real} - \dot{C}_{D,k}^{EN} \tag{22}$$

$$\dot{Z}_k^{EX} = \dot{Z}_k^{real} - \dot{Z}_k^{EN} \tag{23}$$

The unavoidable exergy destruction and investment cost rates are calculated using Eqs. (24) and (25), respectively [30-32]:

$$\dot{C}_{D,k}^{UN} = c_{F,k}^{real}\dot{E}x_{D,k}^{UN} \tag{24}$$

$$\dot{Z}_k^{UN} = \dot{E}x_{P,k}^{real}\left(\frac{\dot{Z}}{\dot{E}x_P}\right)_k^{UN} \quad (25)$$

The minimum values of $(\dot{Z}/\dot{E}x_P)_k^{UN}$ are obtained by applying some assumptions listed in Table 1.

Similarly, the avoidable subdivisions of the cost rates are obtained by Eq. (26) and (27) [30-32]:

$$\dot{C}_{D,k}^{AV} = \dot{C}_{D,k} - \dot{C}_{D,k}^{UN} \quad (26)$$

$$\dot{Z}_k^{AV} = \dot{Z}_k - \dot{Z}_k^{UN} \quad (27)$$

The unavoidable endogenous/exogenous parts of cost rates within the kth component are calculated by Eqs. (28)-(29) [30-32]:

$$\dot{C}_{D,k}^{UN,EN} = c_{F,k}^{real}\,\dot{E}x_{D,k}^{UN,EN} \quad (28)$$

$$\dot{C}_{D,k}^{UN,EX} = \dot{C}_{D,k}^{UN} - \dot{C}_{D,k}^{UN,EN} \quad (29)$$

$$\dot{Z}_k^{UN,EN} = \dot{E}x_{P,k}^{EN}\left(\frac{\dot{Z}}{\dot{E}x_P}\right)_k^{UN} \quad (30)$$

$$\dot{Z}_k^{UN,EX} = \dot{Z}_k^{UN} - \dot{Z}_k^{UN,EN} \quad (31)$$

Finally, the avoidable endogenous/exogenous parts of the cost rates within the kth component are calculated by Eqs. (32)-(35) [30-32]:

$$\dot{C}_{D,k}^{AV,EN} = \dot{C}_{D,k}^{EN} - \dot{C}_{D,k}^{UN,EN} \quad (32)$$

$$\dot{C}_{D,k}^{AV,EX} = \dot{C}_{D,k}^{EX} - \dot{C}_{D,k}^{UN,EX} \quad (33)$$

$$\dot{Z}_k^{AV,EN} = \dot{Z}_k^{EN} - \dot{Z}_k^{UN,EN} \quad (34)$$

$$\dot{Z}_k^{AV,EX} = \dot{Z}_k^{EX} - \dot{Z}_k^{UN,EX} \quad (35)$$

4. RESULTS AND DISCUSSION

Tables 2 and 3 indicate outcomes of the conventional and advanced exergy and exergoeconomic analyses for the desired multi-generation system. According to Table 2, the results of exergy analysis show that the condenser 1 with exergy destruction rate of 1193 kW, which is around 32.7 % of the total exergy destruction rate, is dominant followed by the condenser 2 with exergy destruction rate of 536.1 kW. As revealed, the total exergy destruction rate in the conventional analysis is 3657.837 kW in which 53.77 % is related to the fuel exergy and the remaining is related to the product one. The result of the advanced exergy analysis is represented in Table 2. Outcomes clarify that in the condenser 1, heat exchanger 1A, pump 3 and heat exchanger 2C, the exogenous exergy destruction rate is zero owing to the equality of their $\dot{E}x_{D,k}$ and $\dot{E}x_{D,k}^{EN}$ which indicates that these components are not affected by the remaining components under the theoretical conditions. The maximum exogenous exergy destruction rate value by about 59.7 % of $\dot{E}x_{D,tot}^{EX}$ belongs to the condenser 2.

Table 1. Assumptions for calculating the real, theoretical processes and the unavoidable exergy destructions [24, 32, 33].

Component	Parameters	Real conditions	Theoretical conditions	Unavoidable exergy destruction	Unavoidable investment cost
Condenser 2	$\Delta T_{min}(^{o}C) = T_7 - T_{L\_2}$	11	0	6	20
Pump 2	$\eta_{is}(\%)$	85	100	98	80
Heat exchange 2B	$\Delta T_{min}(^{o}C) = T_{13} - T_8$	15	0	5	20
Heat exchange 1C	$\Delta T_{min}(^{o}C) = T_6 - T_9$	10	0	3	20
Heat exchange 2A	$\Delta T_{min}(^{o}C) = T_{G\_4} - T_{11}$	12	0	3	20
Turbine 2	$\eta_{is}(\%)$	85	100	98	80
Pump 1	$\eta_{is}(\%)$	85	100	98	80
Heat exchange 1B	$\Delta T_{min}(^{o}C) = T_{G\_2} - T_3$	10	0	5	20
Heat exchange 1A	$\Delta T_{min}(^{o}C) = T_{G\_2} - T_3$	10	0	5	20
Turbine 1	$\eta_{is}(\%)$	85	100	98	80
Condenser 1	$\Delta T_{min}(^{o}C) = T_6 - T_{L\_3}$	10	0	5	20
Heat exchange 3A	$\Delta T_{min}(^{o}C) = T_{G\_7} - T_{15}$	2	0	1	20
PEM	$\eta_{is}(\%)$	59	100	72	51
Pump 3	$\eta_{is}(\%)$	85	100	98	80
Heat exchange 2C	$\Delta T_{min}(^{o}C) = T_{18} - T_{L\_4}$	5	0	2	20

Table 2. Conventional and advanced exergetic analyses of components.

Components	$\dot{E}x_F$ **(kW)**	$\dot{E}x_P$ **(kW)**	$\dot{E}x_D$ **(kW)**	$\dot{E}x_D^{EN}$ **(kW)**	$\dot{E}x_D^{EX}$ **(kW)**	$\dot{E}x_D^{UN}$ **(kW)**	$\dot{E}x_D^{AV}$ **(kW)**	$\dot{E}x_D^{UN,EN}$ **(kW)**	$\dot{E}x_D^{AV,EN}$ **(kW)**	$\dot{E}x_D^{UN,EX}$ **(kW)**	$\dot{E}x_D^{AV,EX}$ **(kW)**
Condenser 2	3273	2737	536.1	212.6	323.5	301.946	234.154	132.163	80.437	169.783	153.717
Pump 2	24.93	19.07	5.858	4.506	1.352	0.633	5.225	0.482	4.024	0.151	1.201
Heat exchange 2B	2409	2214	195.2	41.19	154.01	116.321	78.879	52.045	-10.855	64.276	89.734
Heat exchange 1C	2311	2043	268.3	317.6	-49.3	603.996	-335.696	202.012	115.588	401.984	-451.284
Heat exchange 2A	2134	1868	265.3	137.6	127.7	573.231	-307.931	241.322	-103.722	331.910	-204.21
Turbine 2	1801	1495	306.1	204.1	102	37.022	269.078	22.674	181.426	14.348	87.652
Pump 1	64.54	53.92	10.62	10.98	-0.36	1.250	9.370	1.233	9.747	0.017	-0.377
Heat exchange 1B	1406	1023	383.2	462.2	-79	366.7	16.5	366.7	95.5	0.00	-79
Heat exchange 1A	507.1	443.5	63.64	63.64	0.00	33.155	30.485	33.155	30.485	0.00	0.00
Turbine 1	1358	1166	191.9	230.8	-38.9	21.671	170.229	27.321	203.479	-5.650	-33.25
Condenser 1	10230	9038	1193	1193	0.00	1161.20	31.792	1161.20	31.792	0.00	0.00
Heat exchange 3A	0.078	0.034	0.044	0.048	-0.004	0.018	0.026	0.031	0.017	-0.013	0.009
PEM	300.2	174.8	125.4	124.7	0.7	70.976	54.424	71.300	53.399	-0.325	1.025
Pump 3	11.98	10.71	1.275	1.275	0.00	0.154	1.121	0.154	1.121	0.00	0.00
Heat exchange 2C	114.7	12.81	101.9	101.9	0.00	68.451	33.449	40.841	61.059	27.610	-27.610
Overall	25945.5	22298.8	3647.83	3106.13	541.69	3356.73	291.10	2352.64	753.497	1004.09	-462.393

Results show that in the heat exchanger 1B the exogenous exergy destruction rate is negative meaning that the increment of the exergy destruction rate of the other components leads to the decrement of the exergy destruction rate within this component. It is observed that 85.2 % of the total exergy destruction rate is endogenous. It is concluded that to increase the efficiency of the overall system, focus should be on decreasing the irreversibilities of the components themselves.

The results of exergy destruction splitting into the avoidable and unavoidable parts indicate that in condenser 1, 97.3 % of exergy destruction rate is unavoidable and only 2.7 % is avoidable. The avoidable exergy destruction rates of the heat exchanger 1C and 2A are negative meaning that the value of the unavoidable part is higher than the real exergy destruction rate. Therefore, the improvement cannot be possible via these components.

Table 3. The conventional and advanced operating cost rates of components.

Components	$\dot{Z}_D + \dot{C}_D$ **($/h)**	$\dot{Z}_D^{EN} + \dot{C}_D^{EN}$ **($/h)**	$\dot{Z}_D^{EX} + \dot{C}_D^{EX}$ **($/h)**	$\dot{Z}_D^{UN} + \dot{C}_D^{UN}$ **($/h)**	$\dot{Z}_D^{AV} + \dot{C}_D^{AV}$ **($/h)**	$\dot{Z}_D^{UN,EN} + \dot{C}_D^{UN,EN}$ **($/h)**	$\dot{Z}_D^{AV,EN} + \dot{C}_D^{AV,EN}$ **($/h)**	$\dot{Z}_D^{UN,EX} + \dot{C}_D^{UN,EX}$ **($/h)**	$\dot{Z}_D^{UN,EX} + \dot{C}_D^{AV,EX}$ **($/h)**
Condenser 2	23.228	9.216	14.012	13.331	9.897	5.835	3.381	7.496	6.516
Pump 2	0.441	0.339	0.102	0.175	0.266	0.133	0.205	0.042	0.061
Heat exchange 2B	2.598	0.556	2.042	1.617	0.981	0.724	-0.168	0.894	1.148
Heat exchange 1C	15.083	17.825	-2.742	33.967	-18.884	11.361	6.465	22.606	-25.348
Heat exchange 2A	12.668	6.563	6.104	27.409	-14.741	11.539	-4.975	15.870	-9.766
Turbine 2	17.031	11.334	5.698	2.661	14.370	1.630	9.704	1.031	4.666
Pump 1	0.808	0.830	-0.022	0.196	0.612	0.194	0.636	0.003	-0.025
Heat exchange 1B	17.215	20.753	-3.538	16.476	0.738	16.476	4.276	0	-3.538
Heat exchange 1A	2.488	2.488	0	1.359	1.129	1.359	1.129	0	0
Turbine 1	11.144	13.426	-2.281	1.456	9.690	1.835	11.590	-0.380	-1.902
Condenser 1	55.621	55.621	0	54.145	1.476	54.145	1.476	0	0
Heat exchange 3A	0.0019	0.0022	-0.0003	0.0008	0.0011	0.0013	0.0008	-0.0006	0.0003
PEM electrolysis	0.488	0.490	-0.002	0.399	0.089	0.401	0.089	-0.002	-0.0004
Pump 3	0.117	0.117	0	0.047	0.071	0.047	0.071	0	0
Heat exchange 2C	5.167	5.132	0.035	3.475	1.692	2.073	3.059	1.402	-1.367
Overall	164.098	144.691	19.407	156.713	7.386	107.752	36.940	48.961	-29.554

Results of the advanced exergy analysis indicate that turbines 1 and 2 with $\dot{E}x_D^{EN,AV}$ values of 181.426 kW and 203.479 kW, respectively have the higher improvement priority in comparison with the remaining components so that improving their technical conditions or substituting them with new ones causes the increment of system efficiency. It is clearly observed that 258.8 % of the avoidable part is endogenous. The higher values of $\dot{E}x_D^{EN,AV}$ compared to $\dot{E}x_D^{AV}$ lead to the negative values for $\dot{E}x_D^{EX,AV}$. The value of $\dot{E}x_D^{EX,AV}$ in condenser 2 with the highest value of $\dot{E}x_D^{EX,AV}$ in the entire system is 1.71 times of $\dot{E}x_D^{EX,AV}$ in heat exchanger 2B which is the second component with great $\dot{E}x_D^{EX,AV}$. Therefore, improving the operation of the other components has a significant effect on decreasing the exergy destruction rate within condenser 2.

Table 3 indicates the conventional and advanced operating cost rates, i.e. $\dot{C}_{D,k} + \dot{Z}_k$, within each component of the system. The high value of $\dot{C}_{D,k} + \dot{Z}_k$ implies the higher effect of component on the overall system cost. Therefore, the focus should be on the components which have the largest operating cost rate. Conventional analysis shows that condenser 1 has the maximum operating cost rate (33.89 % of the total). According to the advanced results, the avoidable operating cost rates of the heat exchangers 1C and 2A are negative which indicate that the unavoidable operating cost rates within these components are higher than the total operating cost rates. The highest values of $\dot{C}_D^{AV} + \dot{Z}^{AV}$ are for turbines 2 and 1 with values of 14.370 \$/h and 9.69 \$/h, respectively.

It is concluded that the performance influence of the component itself on $\dot{C}_{D,tot} + \dot{Z}_{tot}$ is higher than the remaining components. It is clearly observed that the $\dot{C}_D^{EN} + \dot{Z}^{EN}$ value of condenser 1 is 100 % (its exogenous is zero). Therefore, the operating cost rates of the remaining components do not affect this component. The $\dot{C}_D^{AV,EN} + \dot{Z}^{AV,EN}$ part is important to reduce the total operating cost rate of the system. As observed, heat exchanger 1C, turbines 1 and 2 with values of 31.37 %, 26.2 % and 17.5 %, respectively have the highest $\dot{C}_D^{AV,EN} + \dot{Z}^{AV,EN}$. Moreover, the negative values of $\dot{C}_D^{AV,EN} + \dot{Z}^{AV,EN}$ within heat exchangers 2A and 2B indicate that the effect of the total operating cost rate of the remaining components on these components is higher than the operating costs of these components themselves.

Comparing the results of Tables 2 and 3, it may be concluded that turbines 1 and 2 with the highest values of $\dot{E}_D^{AV,EN}$ and $\dot{C}_D^{AV,EN} + \dot{Z}^{AV,EN}$ are the major components to improve the performance of the overall system.

5. PARAMETRICAL STUDY

Parametric analysis based on advanced exergy and exergoeconomic concepts was performed to assess the effect of key parameters, namely, turbine 1 inlet pressure (P_4), mass flow rate of upper cycle ($\dot{m}_{upper}$),and geothermal mass flow rate ($\dot{m}_{geo}$), on the parts of exergy destruction and cost rates of major components.

5.1. The effects of key parameters on various parts of $\dot{E}x_{D,k}$

5.1.1. The effects of turbine 1 inlet pressure, P_4

Fig. 2 indicates the variation of the conventional and advanced exergy destruction rates of major components versus P_4 varying from 1750 kPa to 2950 kPa, while other variables are fixed. Results show that the increment of P_4 has a positive effect on $\dot{E}x_D$ by about 44.54 % due to the decrement of $\dot{E}x_F$. According to Fig. 2-a, the maximum exergy destruction rate of heat exchanger 1C is unavoidable which decreases as P_4 increases, while the avoidable part rises within 42.55 %. Thus, it is concluded that the performance of the desired component can be improved by reducing the irreversiblities. It is revealed that $\dot{E}x_D^{EN}$ value decreases significantly by about 43.03 % as pressure rises because its product exergy remains almost constant while the fuel exergy decreases owing to the decrement of temperature at point 5. Obviously, the value of $\dot{E}x_D^{UN}$ gets 2 times of $\dot{E}x_D$. Because, under unavoidable conditions, although $\dot{E}x_D^{UN}$ has a little value related to $\dot{E}x_D$, the value of $\dot{E}x_P^{UN}$ drops strongly as the pressure increases. It is concluded that the increment of P_4 has a positive impact on the heat exchanger 1C due to the reduction of $\dot{E}x_D^{total}$ and unavoidable irreversibilities.

Fig. 2-b demonstrates the effect of P_4 on the exergy destruction rate parts of heat exchanger 2A. It is clearly observed that the pressure has a negative effect on $\dot{E}x_D^{tot}$ of this component, so that its value may get 1.5 times at 2800 kPa. It is revealed that at the lowest value of pressure, the value of $\dot{E}x_D^{AV}$ is 73.7 kW which drops with considerable slope as pressure increases. As seen from Fig. 2-b, at 2100 kPa, the value of $\dot{E}x_D^{AV}$ starts to become negative due to the high value of $\dot{E}x_D^{UN}$ in comparison with $\dot{E}x_D^{tot}$. For P_4>2050 kPa, the value of $\dot{E}x_D^{EX}$ is lower than the value of endogenous part. Therefore, the increment of pressure causes that the effect of other components on the exergy destruction of this component decreases. Moreover, the unavoidable part of $\dot{E}x_D^{EN}$ is increasing as the pressure rises which indicates the increments in the irreversibilities of the system.

Comparing the results indicates that increasing P_4 has a significant positive impact on the heat exchanger 1A, so that its exergy destruction rate decreases within 71.7 % followed by the heat exchanger 1C with value of 44.54 %. The maximum increment of avoidable part with a value of 42.55 % is for heat exchanger 1C as P_4 rises and $\dot{E}x_D^{EN,AV}$ in heat exchanger 1C falls within 44.09 %.

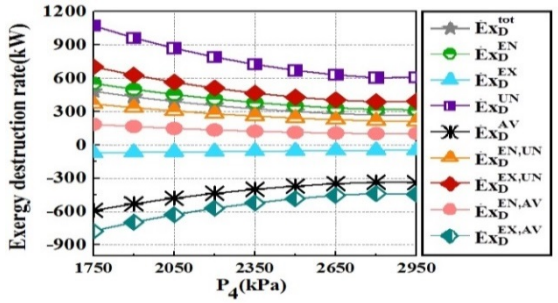

(a) Heat exchanger 1C

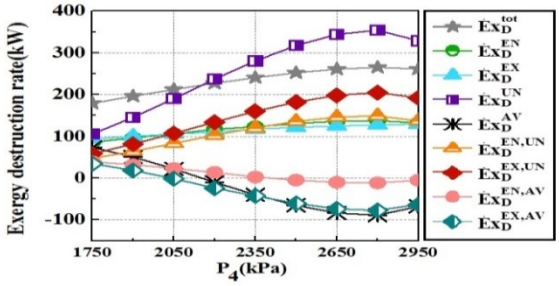

(b) Heat exchanger 2A

Figure 2. The effect of turbine 1 inlet pressure on exergy destruction rate of major components.

5.1.2. The effects of mass rate of upper cycle, $\dot{m}_{upper}$

The effect of $\dot{m}_{upper}$ on the divided exergy destruction rate of the components are plotted in Fig. 3. According to Fig. 3-a, all exergy destruction rates of condenser 2 are decreasing as $\dot{m}_{upper}$ varies from 26 kg/s to 31 kg/s. $\dot{E}x_D^{tot}$ with a value of 50.37 % and $\dot{E}x_D^{EN,AV}$ with a value of 26.63 % have the maximum and the minimum reductions, respectively. As clearly observed, the value of $\dot{E}x_D^{UN}$ is higher than $\dot{E}x_D^{AV}$ for all values of $\dot{m}_{upper}$ but at 30 kg/s, their difference decreases. The value of $\dot{E}x_D^{UN}$ decreases with high slope up to 30 kg/s and then its slope becomes moderate because the value of $\dot{E}x_{P,k}$ decreases significantly at 30 kg/s. It is revealed that $\dot{E}x_D^{EX,AV}$ decreases by about 45 % as $\dot{m}_{upper}$ rises. Therefore, for improvement of exergy potential of this component, focus should be on other components.

The various parts of exergy destruction rates for heat exchanger 2A is illustrated in Fig. 3-b. As observed, the value of unavoidable part of $\dot{E}x_D^{total}$ is the highest leading to the negative values for $\dot{E}x_D^{AV}$ and the maximum and the minimum values of $\dot{E}x_D^{UN}$ and $\dot{E}x_D^{AV}$ occur at 26 kg/s, respectively. Thus, at this value, the component experiences the greatest irreversibilities. Outcomes indicate that the value of real exergy destruction rate decreases by about 25.76 % as the upper mass flow rate increases. Moreover, $\dot{E}x_D^{EN}$ is decreasing because the temperature difference of all points except point 10 decreases relative to the reference temperature and due to the reduction of mass flow rate at bottom cycle (points 10 and 11), the fuel exergy rate decreases significantly and affects the endogenous and real exergy destruction rate.

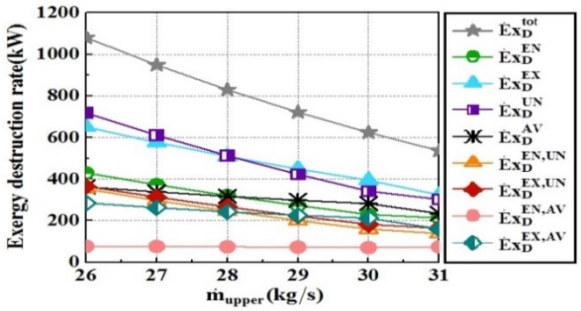

(a) Condenser 2

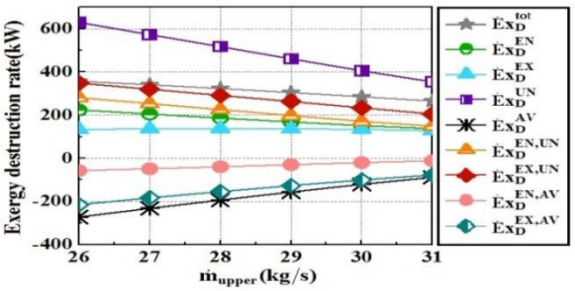

(b) Heatexchanger 2A

Figure 3. The effect of upper cycle mass flow rate on exergy destruction rate of major components.

5.1.3. Geothermal mass flow rate $\dot{m}_{geo}$

Fig. 4 shows the effect of $\dot{m}_{geo}$ on the exergy destruction rate elements for major components. According to Fig. 4-a, all exergy destruction rate parts are decreasing in condenser 2 with $\dot{m}_{geo}$ growth. The maximum exergy destruction rate belongs to $\dot{E}x_D^{tot}$ within 14.84 % because the reduction of fuel exergy due to the decrement of enthalpy and entropy differences is higher than the product by increasing $\dot{m}_{geo}$. About 46.61 % of $\dot{E}x_D^{tot}$ is avoidable decreasing within 14.85 % as $\dot{m}_{geo}$ rises from 17 to 24 kg/s. Thus, the improvement chance of the component reduces with $\dot{m}_{geo}$ growth. Further results indicate that the endogenous part is higher than the exogenous one. Although both of them are decreasing, the reduction percentage of $\dot{E}x_D^{EN}$, relative to its first value, is within 5.5 times of $\dot{E}x_D^{EX}$ reduction. The minimum value of exergy destruction rate is for $\dot{E}x_D^{EN,AV}$ decreasing by about 28.3 %. Therefore, $\dot{m}_{geo}$ increment does not provide improvement chance via the component itself.

As shown in Fig. 4-b, $\dot{E}x_D^{tot}$ of the heat exchanger 1C increases from 262.1 kW to 325.2 kW as $\dot{m}_{geo}$ grows because, the fuel and product exergy rates decrease due to the decrement of mass flow rate at points 9 and 10 as well as the increment of fuel and product difference. This reason is valid for the variation of $\dot{E}x_D^{EN}$. According to the results, $\dot{E}x_D^{EN} > \dot{E}x_D^{tot}$. Thus, the most irreversibilities are due to the component itself. It is clearly observed that the improvement potential of the heat exchanger 1C decreases as $\dot{m}_{geo}$ grows.

As observed from Fig. 4-c, the behavior of exergy destruction rates in heat exchanger 2A are more complex as $\dot{m}_{geo}$ increases. The mass flow rate at points 10 and 11 decrease and all points' temperatures increase with growth of $\dot{m}_{geo}$. These variations elevate the fuel and product exergy rates and thus causes the increment in real exergy destruction rate. For 17 kg/s< $\dot{m}_{geo}$ <20 kg/s, the value of $\dot{E}x_D^{tot}$ grows within 5.37 %, for 20 kg/s< $\dot{m}_{geo}$ < 21 kg/s, the slope is significant and for $\dot{m}_{geo}$ >21 kg/s, the slight slop is observed. Totally, $\dot{E}x_D^{tot}$ increases within 62.23 %. At 20 kg/s, the negative value of $\dot{E}x_D^{AV}$ becomes positive.

Thus, although the real exergy destruction rate increases, the component can be further improved due to the increment of avoidable part. At the maximum value of $\dot{m}_{geo}$, the value of $\dot{E}x_D^{AV}$ and $\dot{E}x_D^{tot}$ are almost equal indicating the high improvement capability of this component at this mass flow rate. $\dot{E}x_D^{EN,AV}$ rises up to 21 kg/s and then decreases and its value becomes positive for $\dot{m}_{geo}$ >20 kg/s.

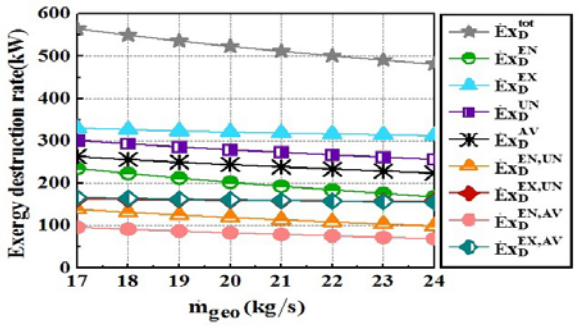

(a) Condenser 2

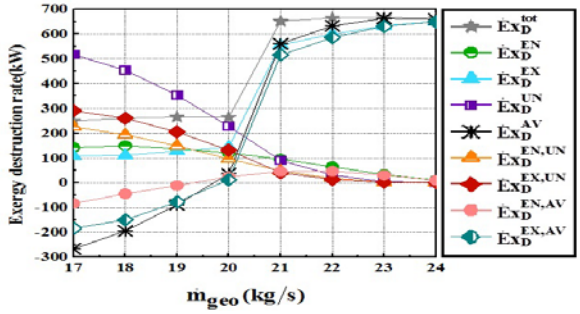

(b) Heat exchanger 2A

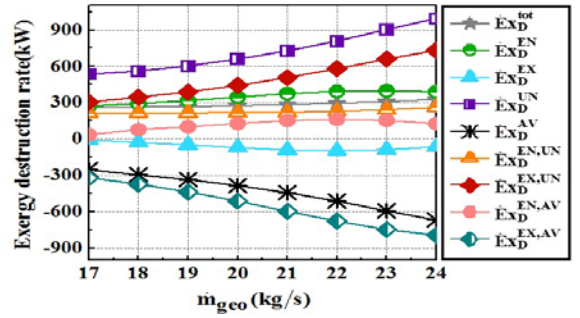

(c) Heat exchanger 1C

Figure 4. The effect of geothermal mass flow rate on exergy destruction rate of major components.

5.2. The effects of key parameters on various parts of $\dot{C}_{D,k} + \dot{Z}_k$

5.2.1. The effect of turbine 1 inlet pressure, P_4

Fig. 5-a illustrates the effect of P_4 on the cost rates of the heat exchanger 1C. It is obvious that the cost rates, which is 99 % of $\dot{C}_D^{tot} + \dot{Z}^{tot}$ is affected by $\dot{C}_{D,k}^{tot}$, drops from 26.76 \$/h to 15.03 \$/h due to the lowering the temperature differences as P_4 increases. The maximum value of the cost rates part is $\dot{C}_D^{UN} + \dot{Z}^{UN}$ decreasing within 42.72 % because the exergy destruction rate drops while c_f grows within 1.15 %. Moreover, as mentioned in Fig. 2-a, $\dot{E}x_D^{UN}$ decreases by 43.45 %. Hence, according to $\dot{C}_{D,k}^{UN} = c_{F,k}^{real} \dot{E}x_{D,k}^{UN}$, $\dot{C}_{D,k}^{UN}$ and also, $\dot{Z}^{UN}$ decrease.

As observed from Fig. 5-b, the value of $\dot{C}_D^{tot} + \dot{Z}^{tot}$ in heat exchanger 2A increases 31 % up to 2800kPa and then decreases within 14.9 % up to the end. This behavior is the function of the variation of $\dot{E}x_D^{tot}$ explained in Fig. 2-b. 99.33 % of the cost rates is related to the $\dot{C}_D^{tot}$ depending on $\dot{E}x_D^{tot}$ and the remaining portion is $\dot{Z}^{tot}$ dropping within 3.2 % due to the decrement of the heat exchanger area ($\dot{Z}$ is the function of the heat exchanger area [34]) as P_4 increases. It is clearly observed that both endogenous and exogenous cost rates is increasing by 33.45 % and 26.47 %, respectively with growth of P_4. Therefore, it is concluded that the cost rates are due to the component itself. Up to 2050kPa, $\dot{C}_D^{UN} + \dot{Z}^{UN} < \dot{C}_D^{tot} + \dot{Z}^{tot}$ and for P_4> 2200kPa the unavoidable cost rates get higher. The avoidable part is decreasing up to 2800 kPa and becomes negative from 2050kPa. This shows the negative effect of P_4 on the improvement potential. The decrement of $\dot{C}_D^{EN,AV} + \dot{Z}^{EN,AV}$ with P_4 growth indicates the reduction of improving the system via this component.

According to the obtained results, the value of avoidable cost rates is little (about 6.5 % of $\dot{C}_D^{tot} + \dot{Z}^{tot}$) decreasing as P_4 drops due to the decrement of both $\dot{C}_D^{AV}$ and $\dot{Z}^{AV}$. $\dot{C}_D^{AV}$ reduction depends on the behavior of $\dot{E}_D^{AV}$ explained in Fig. 2-c and $\dot{Z}^{AV}$ reduction is due to the increase of the heat exchanger area under the unavoidable conditions. Taking the results together, it is revealed that the growth of P_4 from1750kPa to 2950kPa causes the decrement of cost rates only in the heat exchanger 1C. In the heat exchanger 1C, $\dot{C}_D^{AV} + \dot{Z}^{AV}$ is negative with 41.8 % increment with P_4 increase and it is decreasing in heat exchanger $\dot{C}_D^{EN,AV} + \dot{Z}^{EN,AV}$ and $\dot{C}_D^{EX,AV} + \dot{Z}^{EX,AV}$ in heat exchanger 2A decrease and become negative.

5.2.2. The effect of mass rate of upper cycle, $\dot{m}_{upper}$

Fig. 6 illustrates the behavior of cost rates in major components when $\dot{m}_{upper}$ varies from 26 kg/s to 31kg/s. According to Fig. 6-a, all parts of cost rates in the condenser 2 are decreasing as $\dot{m}_{upper}$ increases. $\dot{C}_D^{tot} + \dot{Z}^{tot}$

has the maximum reduction (50.27 %) due to the decrement of $\dot{C}_D^{tot}$ as well as $\dot{Z}^{tot}$ referring to the decrement of the exergy destruction rate and $\dot{m}_{13}$, respectively. Results represent that $\dot{C}_D^{AV}+\dot{Z}^{AV}$ drops within 40.41 % and it has a drastic reduction for $\dot{m}_{upper}$ >30kg/s indicating the weakness of improvement potential of this component for the higher value of $\dot{m}_{upper}$.

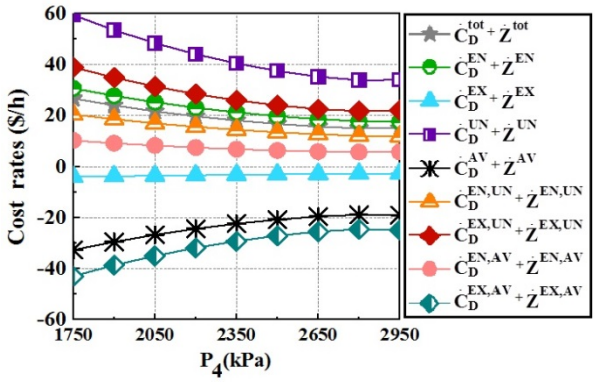

(a) Heat exchanger 1C

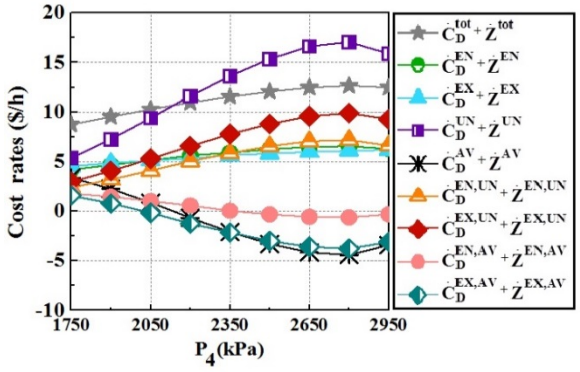

(b) Heat exchanger 2A

Figure 5. The effect of turbine 1 inlet pressure on cost rates of major components.

5.2.3. Geothermal mass flow rate $\dot{m}_{geo}$

Fig. 7-a depicts the cost rate variations of condenser 2 when $\dot{m}_{geo}$ is supposed to change from 17kg/s to 24kg/s. Outcomes indicate that $\dot{C}_D^{tot}+\dot{Z}^{tot}$ is maximum while $\dot{C}^{EN,AV}+\dot{Z}^{EN,AV}$ is minimum and all cost rates part with positive values are decreasing with $\dot{m}_{geo}$ growth. $\dot{C}_D^{tot}+\dot{Z}^{tot}$ shows 14.84 % reduction due to decrement of both $\dot{C}_D^{tot}$ (owing to the reduction of exergy destruction rate) and $\dot{Z}^{tot}$ (owing to decrement of bottom cycle mass flow rate). 38.57 % of $\dot{C}_D^{tot}+\dot{Z}^{tot}$ is related to $\dot{C}_D^{EN}+\dot{Z}^{EN}$ indicating the strong interactions among the remaining components. The value of $\dot{C}_D^{AV}+\dot{Z}^{AV}$ decreases about 15.71 % at which $\dot{C}_D^{EN,AV}+\dot{Z}^{EN,AV}$ has the more reduction (29.27 %) than $\dot{C}_D^{EX,AV}+\dot{Z}^{EX,AV}$ (7.9 %) with growth of $\dot{m}_{geo}$. As clearly revealed from Fig. 7-b, in heat exchanger 1C, $\dot{Z}^{tot}$ and $\dot{C}_D^{tot}$ increases due to increment of the heat transfer area and the exergy destruction rate within 24.38 % and 27.98 %, respectively causing the growth of $\dot{C}_D^{tot}+\dot{Z}^{tot}$ from 14.58$/h to 18.66$/h as $\dot{m}_{geo}$ rises. Further results indicate that $\dot{C}_D^{AV}+\dot{Z}^{AV}$, $\dot{C}_D^{EX,AV}+\dot{Z}^{EX,AV}$ are decreased with $\dot{m}_{geo}$ growth and $\dot{C}_D^{EN,AV}+\dot{Z}^{EN,AV}$ has a drastic increment due to 48.4 % increase of $\dot{C}_D^{EN}+\dot{Z}^{EN}$. According to Fig. 7-c, $\dot{C}_D^{tot}+\dot{Z}^{tot}$ in heat exchanger 2A increases slightly up to 20kg/s and has a drastic increase between 20kg/s and 21kg/s and then a slight increment is observed. Generally, $\dot{C}_D^{tot}+\dot{Z}^{tot}$ increases within 51.67 % as $\dot{m}_{geo}$ grows. $\dot{C}_D^{AV}+\dot{Z}^{AV}$, $\dot{C}_D^{AV,EN}+\dot{Z}^{AV,EN}$ and $\dot{C}_D^{AV,EX}+\dot{Z}^{AV,EX}$ increase sharply so that at 24kg/s $\dot{C}_D^{UN}+\dot{Z}^{UN}$ approaches zero and $\dot{C}_D^{AV}+\dot{Z}^{AV}$ has a little difference with the real cost rates. According to the growth of $\dot{C}_D^{AV,EX}+\dot{Z}^{AV,EX}$, it is concluded that improving the cost rates of this component depends on the remaining components improvement.

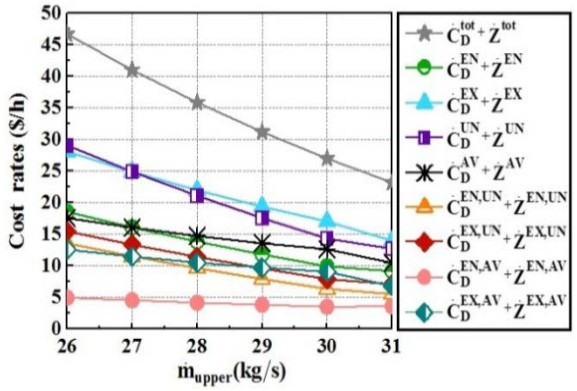

(a) Condenser 2

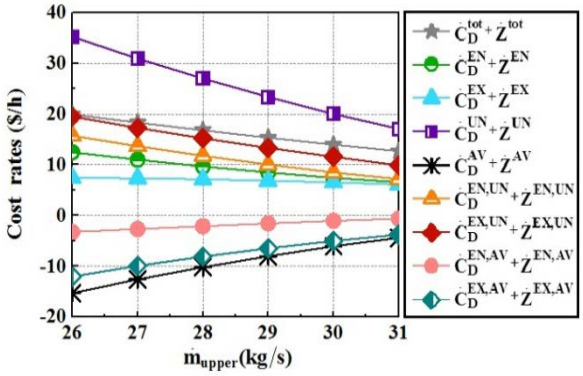

(b) Heat exchanger 2A

Figure 6. The effect of upper cycle mass flow rate on cost rates of major components.

According to the obtained results, the increase of $\dot{m}_{geo}$ has a positive effect on $\dot{C}_D^{tot}+\dot{Z}^{tot}$ in condenser 2 within 14.8 %. Moreover, $\dot{C}_D^{AV}+\dot{Z}^{AV}$ rises for heat exchanger 2A by 18.25 %. In addition, $\dot{C}_D^{EN,AV}+\dot{Z}^{EN,AV}$ in heat exchanger 1C increases within 130.5 % as $\dot{m}_{geo}$ rises.

6. CONCLUSIONS

Within the scope of this work. For the first time, a new geothermal multi-generation system with a major part of LNG regasification cycle is proposed and analyzed based on the conventional and advanced exergy and exergoeconomic concepts. The effect of key parameters namely, P_4, $\dot{m}_{upper}$ and $\dot{m}_{geo}$ on the exergy destruction and cost rates subdivisions of the system components are performed. The main conclusion from the outcomes of the present work may be summarized as follows:

- The increment of P_4 improves the avoidable parts of total exergy and cost rates of heat exchanger 1C within 42.55 % and 41.8 %, respectively among all components.
- With growth of $\dot{m}_{upper}$, total exergy and cost rates of condenser 2 reduce respectively by about 50.37 % and 50.27 % and the maximum improvement of avoidable cost rates is obtained by 71.22 % for heat exchanger 2A.

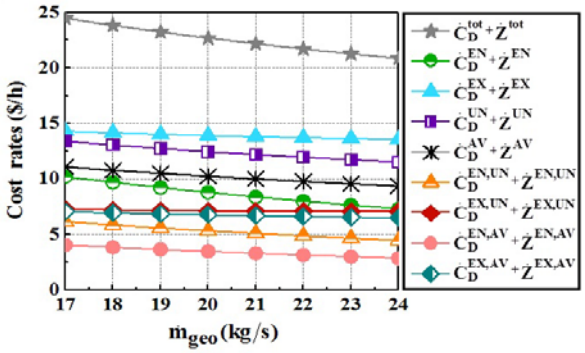

(a) Condenser C-2

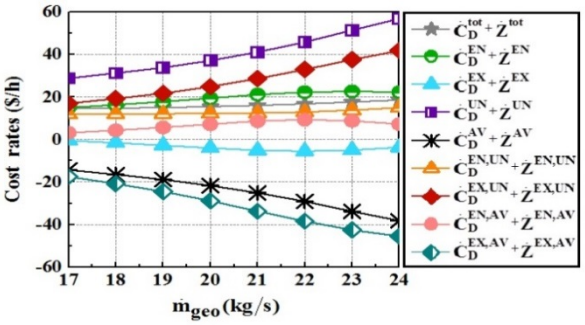

(b) Heat exchanger H_1C

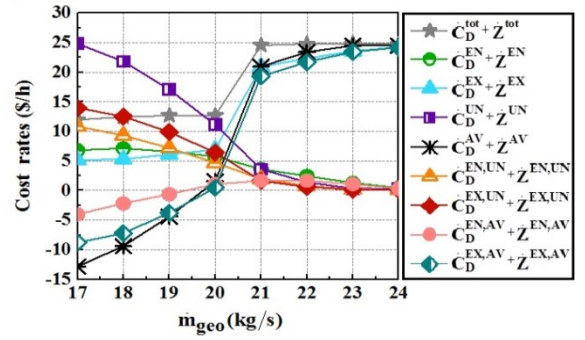

(c) Heat exchanger 2A

Figure 7. The effect of geothermal mass flow rate on cost rates of major components.

As $\dot{m}_{geo}$ grows, the maximum decrement in the exergy destruction rate occurs in condenser 2 by 14.84 %. In heat exchanger 2A, the avoidable and endogenous avoidable parts increase from -266.36 kW to 659.41kW and 93.54 %, respectively. Moreover, the total cost rates of condenser 2 is improved by 14.8 %.

7. ACKNOWLEDGMENT

Authors would like to thank all Alzahra University to supporting this research.

REFERENCES

1. Ratlamwala, T., Dincer, I.T. and Gadalla, M., "Performance analysis of a novel integrated geothermal-based system for multi-generation applications", ***Applied Thermal Engineering***, Vol. 40, (2012), 71-79. (https://doi.org/10.1016/j.applthermaleng. 2012.01.056).
2. Coskun, C., Oktay, Z. and Dincer, I., "Thermodynamic analyses and case studies of geothermal based multi-generation systems", ***Journal of Cleaner Production***, Vol. 32, (2012), 71-80. (https://doi.org/10.1016/j.jclepro.2012.03.004).
3. Ozturk, M. and Dincer, I., "Thermodynamic analyses and case studies of geothermal based multi-generation systems", ***Applied Thermal Engineering***, Vol. 51, (2013), 1235-1244. (https://doi.org/10.1016/j.jclepro.2012.03.004).
4. Ratlamwala, T. and Dincer, I., "Development of a geothermal based integrated system for building multigenerational needs", ***Energy and Buildings***, Vol. 62, (2013), 496-506. (https://doi.org/10.1016/j.enbuild.2013.03.004).
5. Al-Ali, M. and Dincer, I., "Energetic and exergetic studies of a multigenerational solar–geothermal system", ***Applied Thermal Engineering***, Vol. 71, (2014), 16-23. (https://doi.org/10.1016/ j.applthermaleng.2014.06.033).
6. Suleman, F., Dincer, I. and Agelin-Chaab, M., "Development of an integrated renewable energy system for multigeneration", ***Energy***, Vol. 78, (2014), 196-204. (https://doi.org/10.1016/ j.energy.2014.09.082).
7. Malik, M., Dincer, I. and Rosen, M.A., "Development and analysis of a new renewable energy-based multi-generation system", ***Energy***, Vol. 79, (2015), 90-99. (https://doi.org/ 10.1016/j.energy.2014.10.057).
8. Khalid, F., Dincer, I. and Rosen, M.A., "Energy and exergy analyses of a solar-biomass integrated cycle for multigeneration", ***Solar Energy***, Vol. 112, (2015), 290-299. (https://doi.org/10.1016/j.solener.2014.11.027).
9. Panchal, S., Dincer, I. and Agelin-Chaab, M., "Analysis and evaluation of a new renewable energy based integrated system for residential applications", ***Energy and Buildings***, Vol. 128, (2016), 900-910. (https://doi.org/10.1016/j.enbuild.2016. 07.038).
10. Almahdi, M., Dincer, I. and Rosen, M.A., "A new solar based multigeneration system with hot and cold thermal storages and hydrogen production", ***Renewable Energy***, Vol. 91, (2016), 302-314. (https://doi.org/10.1016/j.renene.2016.01.069).
11. Ahmadi Boyaghchi, F. and Nazer, S.,"Assessment and optimization of a new sextuple energy system incorporated with concentrated photovoltaic thermal - Geothermal using exergy, economic and environmental", ***Journal of Cleaner Production,*** Vol. 165, (2017), 70-84. (https://doi.org/10.1016/j.jclepro. 2017.06.194).
12. Ahmadi Boyaghchi, F. and Chavoshi, M.I., "Multi-generation system incorporated with PEM electrolyzer and dual ORC based on biomass gasification waste heat recovery: Exergetic, economic and environmental impact optimizations", ***Energy***, Vol. 145, (2018), 38-51. (https://doi.org/10.1016/j.energy. 2017.12.118).

13. Tsatsaronis, G., Design optimization using exergoeconomics, in Thermodynamic optimization of complex energy systems, Springer, (1999), 101-115.
14. Bejan, A. and Tsatsaronis, G., Thermal design and optimization, John Wiley & Sons, (1996).
15. Moharamian, A., Soltani, S., Rosen, M.A. and Mahmoudi, S.M.S., "Advanced exergy and advanced exergoeconomic analyses of biomass and natural gas fired combined cycles with hydrogen production. Applied Thermal Engineering", ***Applied Thermal Engineering***, Vol. 134, (2018), 1-11. (https://doi.org/10.1016/j.applthermaleng.2018.01.103).
16. Tsatsaronis, G., Strengths and limitations of exergy analysis, in Thermodynamic optimization of complex energy systems, Springer, (1999), 93-100.
17. Tsatsaronis, G., "Recent developments in exergy analysis and exergoeconomics", ***International Journal of Exergy***, Vol. 5, (2008), 489-499. (https://doi.org/10.1504/IJEX.2008.020822).
18. Petrakopoulou, F., Tsatsaronis, G., Morosuk, T. and Carassai, A., "Conventional and advanced exergetic analyses applied to a combined cycle power plant", ***Energy***, Vol. 41, (2012), 146-152. (https://doi.org/10.1016/j.energy.2011.05.028).
19. Asgari, S., Noorpoor, A.R. and Ahmadi Boyaghchi, F., "Parametric assessment and multi-objective optimization of an internal auto-cascade refrigeration cycle based on advanced exergy and exergoeconomic concepts", ***Energy***, Vol. 125, (2017), 576-590. (https://doi.org/10.1016/j.energy.2017.02.158).
20. Mehrpooya, M. and Mousavi, S.A., "Advanced exergoeconomic assessment of a solar-driven Kalina cycle", ***Energy Conversion and Management***, Vol. 178, (2018), 78-91. (https://doi.org/10.1016/j.enconman.2018.10.033).
21. Khosravi, H., Salehi, G.R., and Azad, M.T., "Design of structure and optimization of organic Rankine cycle for heat recovery from gas turbine: The use of 4E, advanced exergy and advanced exergoeconomic analysis", ***Applied Thermal Engineering***, Vol. 147, (2019), 272-290. (https://doi.org/10.1016/j.applthermaleng.2018.09.128).
22. Ahmadi Boyaghchi, F. and Safari, H., "Parametric study and multi-criteria optimization of total exergetic and cost rates improvement potentials of a new geothermal based quadruple energy system", ***Energy Conversion and Management***, Vol. 137, (2017), 130-141. (https://doi.org/10.1016/j.enconman.2017.01.047).
23. Xue, X., Guo, C., Du, X., Yang, L. and Yang, Y., "Thermodynamic analysis and optimization of a two-stage organic Rankine cycle for liquefied natural gas cryogenic exergy recovery", ***Energy***, Vol. 83, (2015), 778-787. (https://doi.org/10.1016/j.energy.2015.02.088).
24. Ahmadi Boyaghchi, F. and Molaie, H., "Sensitivity analysis of exergy destruction in a real combined cycle power plant based on advanced exergy method", ***Energy Conversion and Management***, Vol. 99, (2015), 374-386. (https://doi.org/10.1016/j.enconman.2015.04.048).
25. Ahmadi, P., Dincer, I. and Rosen, M.A., "Energy and exergy analyses of hydrogen production via solar-boosted ocean thermal energy conversion and PEM electrolysis", ***International Journal of Hydrogen Energy***, Vol. 38, (2013), 1795-1805. (https://doi.org/10.1016/j.ijhydene.2012.11.025).
26. Kelly, S., Tsatsaronis, G. and Morosuk, T., "Advanced exergetic analysis: Approaches for splitting the exergy destruction into endogenous and exogenous parts", ***Energy***, Vol. 34, (2009), 384-391. (https://doi.org/10.1016/j.energy.2008.12.007).
27. Tsatsaronis, G. and Park, M.-H., "On avoidable and unavoidable exergy destructions and investment costs in thermal systems", ***Energy Conversion and Management***, Vol. 43, (2002), 1259-1270. (https://doi.org/10.1016/S0196-8904(02)00012-2).
28. Tsatsaronis, G., Cziesla, F. and Gao, Z., "Avoidable Thermodynamic Inefficiencies and Costs in Energy Conversion Systems. Part 1: Methodology", ***Proceedings of ECOS***, Vol. 2, (2003), 809-814.
29. Vučković, G.D., et al., "Advanced exergy analysis and exergoeconomic performance evaluation of thermal processes in an existing industrial plant", ***Energy Conversion and Management***, Vol. 85, (2014), 655-662. (https://doi.org/10.1016/j.enconman.2014.03.049).
30. Keçebaş, A. and Hepbasli, A., "Conventional and advanced exergoeconomic analyses of geothermal district heating systems", ***Energy and Buildings***, Vol. 69, (2014), 434-441. (https://doi.org/10.1016/j.enbuild.2013.11.011).
31. Anvari, S., Saray, R.K. and Bahlouli, K., "Conventional and advanced exergetic and exergoeconomic analyses applied to a tri-generation cycle for heat, cold and power production", ***Energy***, Vol. 91, (2015), 925-939. (https://doi.org/10.1016/j.energy.2015.08.108).
32. Açıkkalp, E., Aras, H. and Hepbasli, A., "Advanced exergoeconomic analysis of an electricity-generating facility that operates with natural gas", ***Energy Conversion and Management***, Vol. 78, (2014), 452-460. (https://doi.org/10.1016/j.enconman.2013.11.003).
33. Petrakopoulou, F., Tsatsaronis, G. and Morosuk, T., "Evaluation of a power plant with chemical looping combustion using an advanced exergoeconomic analysis", ***Sustainable Energy Technologies and Assessments***, Vol. 3, (2013), 9-16. (https://doi.org/10.1016/j.seta.2013.05.001).
34. El-Emam, R.S. and Dincer, I., "Exergy and exergoeconomic analyses and optimization of geothermal organic Rankine cycle", ***Applied Thermal Engineering***, Vol. 59, (2013), 435-444. (https://doi.org/10.1016/j.applthermaleng.2013.06.005).